International Journal of Nanomedicine

Dovepress
open access to scientific and medical research

Open Access Full Text Article

ORIGINAL RESEARCH

The Synergistic Effect of Hyperthermia and Chemotherapy in Magnetite Nanomedicine-Based Lung Cancer Treatment

This article was published in the following Dove Press journal:
International Journal of Nanomedicine

Shu-Jyuan Yang[1]
Chung-Huan Huang[1]
Chung-Hao Wang[2]
Ming-Jium Shieh[1,3]
Ke-Cheng Chen[1,4]

[1]Institute of Biomedical Engineering, College of Medicine and College of Engineering, National Taiwan University, Taipei, Taiwan; [2]Gene'e Tech Co. Ltd., New Taipei City, Taiwan; [3]Department of Oncology, National Taiwan University Hospital and College of Medicine, Taipei, Taiwan; [4]Department of Surgery, National Taiwan University Hospital and College of Medicine, Taipei, Taiwan

Background: Lung cancer is the leading cause of cancer patient death in the world. There are many treatment options for lung cancer, including surgery, radiation therapy, chemotherapy, targeted therapy, and combined therapy. Despite significant progress has been made in the diagnosis and treatment of lung cancer during the past few decades, the prognosis is still unsatisfactory.

Purpose: To resolve the problem of chemotherapy failure, we developed a magnetite-based nanomedicine for chemotherapy acting synergistically with loco-regional hyperthermia.

Methods: The targeting carrier consisted of a complex of superparamagnetic iron oxide (SPIO) and poly(sodium styrene sulfonate) (PSS) at the core and a layer-by-layer shell with cisplatin (CDDP), together with methotrexate – human serum albumin conjugate (MTX −HSA conjugate) for lung cancer-specific targeting, referred to hereafter as SPIO@PSS/CDDP/HSA−MTX nanoparticles (NPs).

Results: SPIO@PSS/CDDP/HSA−MTX NPs had good biocompatibility and stability in physiological solutions. Furthermore, SPIO@PSS/CDDP/HSA−MTX NPs exhibited a higher temperature increase rate than SPIO nanoparticles under irradiation by a radiofrequency (RF) generator. Therefore, SPIO@PSS/CDDP/HSA−MTX NPs could be used as a hyperthermia inducer under RF exposure after nanoparticles preferentially targeted and then accumulated at tumor sites. In addition, SPIO@PSS/CDDP/HSA−MTX NPs were developed to be used during combined chemotherapy and hyperthermia therapy, exhibiting a synergistic anticancer effect better than the effect of monotherapy.

Conclusion: Both in vitro and in vivo results suggest that the designed SPIO@PSS/CDDP/HSA−MTX NPs are a powerful candidate nanoplatform for future antitumor treatment strategies.

Keywords: lung cancer, hyperthermia, chemotherapy, superparamagnetic iron oxide nanoparticles, cisplatin, methotrexate

Introduction

Lung cancer is the main cause of cancer death and can be divided into small cell carcinoma (10–15%) and non-small cell carcinoma (85–90%), which includes adenocarcinoma, linear cell carcinoma, and large cell carcinoma. Lung cancer's pathogenic risk factors include smoking, environmental toxins, age, and heredity. Metastatic disease is observed in about 40% of newly diagnosed patients with non-small cell carcinoma, and most of the remainders eventually develop into metastases.[1,2] Despite new advances in lung cancer treatment in the past few

Correspondence: Ke-Cheng Chen
Tel +886-2-23123456 ext 65077
Email 010288@ntuh.gov.tw

submit your manuscript | www.dovepress.com
DovePress
http://doi.org/10.2147/IJN.S281029

decades, the prognosis of lung cancer is still not idea, and the overall 5-year survival rate remains low.[3] Therefore, it is essential to develop new novel therapeutic approaches to improve the prognosis of lung cancer.

Cisplatin, also known as cisplatinum, cis-diamminedichloroplatinum (II), and CDDP, is a well-known chemotherapeutic drug used to treat a number of cancers, including cancers of the lung, ovary, germ cells, head and neck, bladder, cervix, and endometrium.[4] Although its anticancer effect is good, patients often find CDDP treatment unacceptable or even give up treatment due to serious side effects.[5] In order to solve these serious side effects of CDDP, a new generation of platinum-based chemotherapy drugs, such as oxaliplatin and carboplatin, has been successively developed. However, high therapy cost limits the substitution of CDDP in chemotherapeutic drugs. Therefore, extensive efforts worldwide have been made to find an improved CDDP carrier. It has been demonstrated that a mix of anticancer drugs and/or treatment methods enhances treatment efficiency by way of synergistic therapeutic effects and by overcoming drug resistance.[6]

Targeted delivery of proven therapeutic agent directly to cancer cells by cell surface receptors, sparing normal cells, is of current interest in oncologic pharmacology.[7] Recently, several receptors have been evidenced promise as therapeutic targets include epidermal growth factor receptor, interleukin, folate, and integrin αvβ3. These receptors are strongly expressed in brain, lung, breast, colon, ovarian cancers and can be served as physiological target ligands for therapeutic drug delivery.[8–12] Because folic acid is a stable and generally poorly immunogenic chemical with a high affinity toward the folate receptor, it is widely used as a versatile moiety on the surface of drug carriers to provide a targeted delivery of the drug to tumor tissue and efficient folate receptor-mediated endocytosis in cancer cells.[13,14] Methotrexate (MTX), a structural analog of folic acid, is classified in antifolate therapeutic agents used to treat cancers and rheumatoid arthritis by targeting dihydrofolate reductase (DHFR) and thymidylate synthetase to inhibit purine and pyrimidine synthesis.[15] Moreover, MTX can inhibit the specific steps of folic acid metabolism and lead to a depletion of folic acid, which finally provokes cytotoxicity, particularly by preventing DNA synthesis, methylation, and repair.[16] Therefore, MTX is used in dual-acting molecules that can act as a tumor target ligand and a therapeutic agent at the same time.

Body temperature is a balance between heat production and dissipation, increasing when the rate of production exceeds the rate of dissipation. Hyperthermia is the condition in which body temperature rises to a higher level than normal, but also is the name for the carefully controlled use of heat for medical purposes.[17] Because of the abnormal structure of neovascularization in tumor tissues, heating to 40–43°C results in hypoxia, lactic acid accumulation, low pH, and nutrient deficiency in tumor tissues, ultimately causing cancer cell death. The hyperthermia therapy, based on the use of ultrasound, electromagnetic waves, external heating of the chest, or extracorporeal circulation heating is currently in common use in local treatments, such as liver, kidney, and other solid organs, due to the difficulty of controlling the treating temperature beyond 60°C. At present, the use of hyperthermia as an adjuvant therapy is known to effectively increase the sensitivity of cancer cells to chemotherapy and radiotherapy while reducing the discomfort of treatment.[18,19]

Because of the low toxicity and well-known pathways of metabolism, magnetic particles have been widely applied in magnetic resonance imaging (MRI),[20,21] biomedicine,[22,23] drug delivery,[24–27] and hyperthermia therapy.[28–30] Recently, the encouraging results have been achieved in the magnetic particle-based hyperthermia studies,[30–33] but the application in clinical use is still few due to the administration of magnetic particles via the intra-tumor injection,[34–36] which leads to a non-homogeneous nanoparticle distribution within the tumor and is barely potential in the localized and superficial or directly accessible tumor.[37]

The purpose of this study is to develop a highly biocompatible nanoparticle that serves a dual purpose in hyperthermia and chemotherapy for lung cancer treatment. This nanoparticle is based on a complex of superparamagnetic iron oxide (SPIO) and poly(sodium styrene sulfonate) (PSS) at the core, with a layer-by-layer (LbL) coating of CDDP and human serum albumin (HSA) or MTX−HSA conjugate (Scheme 1A). As described herein, the HSA coating can increase the compatibility and half-life of nanoparticles in the blood,[38] while MTX conjugation can increase the NPs' ability to target the tumor biomarker and act as a therapeutic agent. In addition, SPIO nanoparticles can be used as a hyperthermia inducer to improve cancer treatment by generating local heat when exposed to a radiofrequency (RF) generator. Synthesis and testing

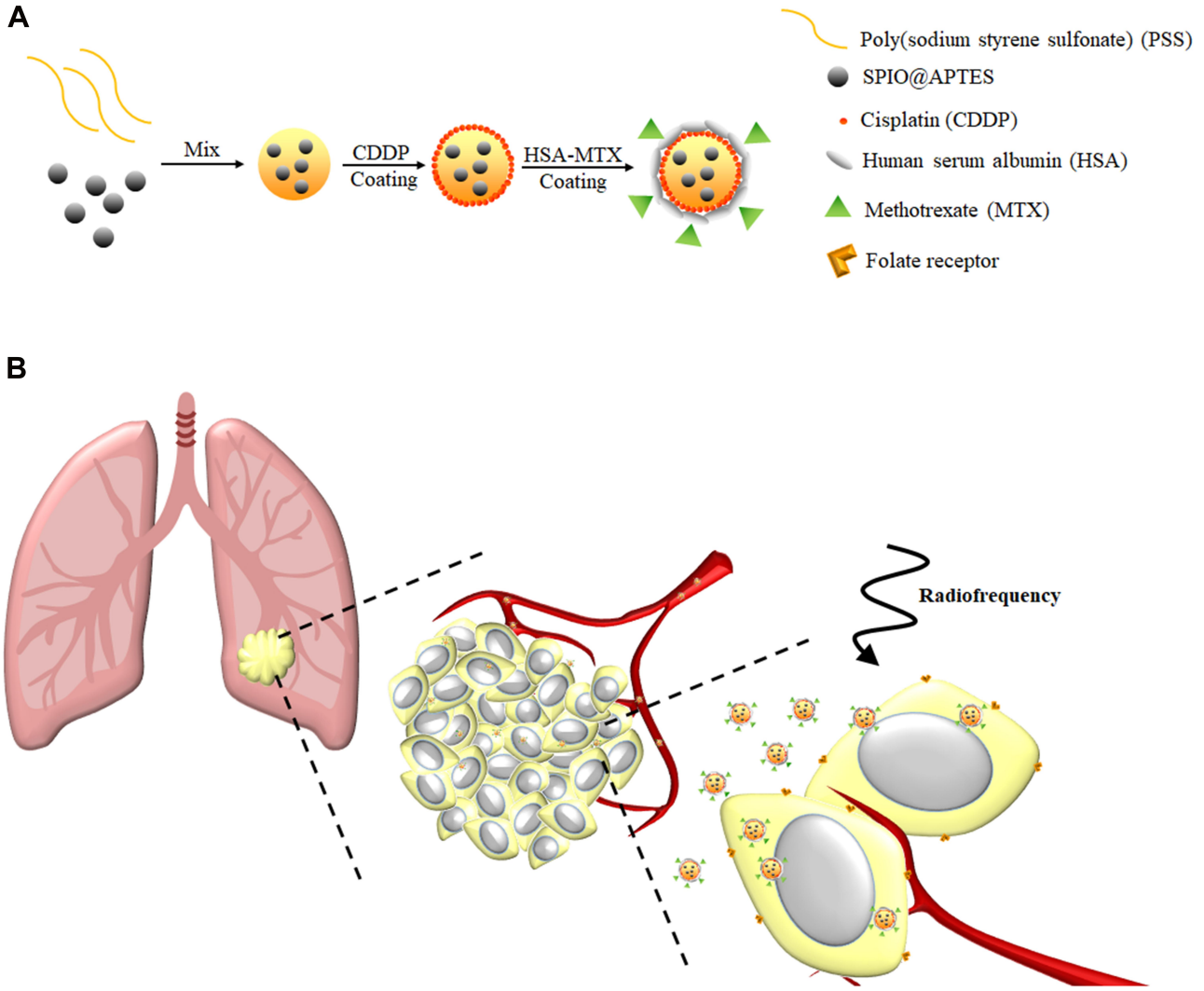

Scheme 1 (**A**) SPIO@PSS/CDDP/HSA−MTX NPs were prepared using the Layer-by-Layer technique. (**B**) Schematic representation of SPIO@PSS/CDDP/HSA−MTX NPs used for lung cancer therapy using loco-regional hyperthermia combined with chemotherapy.

of these NPs were performed in hopes that hyperthermia and chemotherapy involving SPIO@PSS/CDDP/HSA −MTX NPs might become a promising tool for cancer therapy, to kill cancer cells and reduce the probability of tumor recurrence (Scheme 1B).

Materials and Methods

Materials

SPIO and SPIO@(3-aminopropyl)triethoxysilane (APTES) nanoparticles were kindly supplied by Gene'e Tech Co., Ltd. (Taiwan). PSS, CDDP, HSA, anhydrous dimethyl sulfoxide (DMSO), N-(3-Dimethylaminopropyl)-N'-ethylcarbodiimide hydrochloride (EDC), fluorescein 5(6)-isothiocyanate (FITC), and 3-(4,5-dimethylthiazol-2-yl)-2,5-diphenyltetrazolium bromide (MTT) were acquired from Sigma–Aldrich (USA). MTX was purchased from Merck KGaA (Darmstadt, Germany).

Conjugation of MTX with HSA

The conjugation of MTX to HSA molecules was performed as follows: A well-dissolved mixture of MTX and EDC at molar ratio 1:1 in 5 mL anhydrous DMSO was dropped slowly into 5% (w/v) HSA solution (pH 6.5) and stirred at room temperature in the dark for 16 h to allow MTX to conjugate onto HSA molecules. Remaining unreacted MTX molecules in the mixture were moved through a CelluSep dialysis membrane (Membrane Filtration Products, Seguin, TX, USA), which had a molecular weight cut-off of 3.5 kD. Finally, the MTX-conjugated HSA was collected by lyophilization and kept for follow-up study.[14]

Characterization of MTX–HSA Conjugates

The chemical compositions of HSA, MTX–HSA conjugates, and MTX were characterized with an attenuated total reflection (ATR) – FT-IR spectrometer (Thermo Scientific Nicolet 6700; MA, USA). The MTX:HSA molar ratios in MTX–HSA conjugates were estimated by determining the intensity of the absorption maximum (375 nm) of the MTX derivative in MTX–HSA conjugate in 0.01 M NaOH solution with a UV-vis spectrophotometer/microplate reader (SpectraMax Plus, Molecular Devices, USA). Herein, MTX pre-dissolved in 0.01 M NaOH solution was diluted to a series of gradient standard solution for the preparation of calibration curve and further analysis.

Preparation of SPIO@PSS/CDDP/HSA and SPIO@PSS/CDDP/HSA–MTX NPs

SPIO@PSS/CDDP/HSA NPs and SPIO@PSS/CPPD/HSA–MTX NPs were prepared using the LbL technique. First, 5.5 mg of PSS powder was dissolved in 0.55 mL deionized (DI) water, and then vigorously mixed with 1 mL of SPIO@APTES solution (OD_{500} = 0.673 and pH = 7.0) for 2 h to obtain SPIO@PSS NPs. Then, 0.14 mL of 2 mg/mL CDDP solution was vigorously agitated with 1 mL of the SPIO@PSS solution (pH = 5.0) for 2 h to coat CDDP onto SPIO@PSS NPs. Finally, 1 mL of the SPIO@PSS/CDDP NP solution (pH = 6.0) was added into 0.6 mL of HSA or HSA–MTX conjugate in aqueous solution (30 mg/mL, pH = 4.2) and stirred for 2 h to form SPIO@PSS/CDDP/HSA or SPIO@PSS/CDDP/HSA–MTX NPs. In order to remove free HSA or HSA–MTX conjugate, the prepared SPIO@PSS/CDDP/HSA or SPIO@PSS/CDDP/HSA–MTX NP solutions were centrifuged at 20,000 g for 10 min, and the precipitates were re-dispersed in DI water and stored at 4°C until use.

Characterization of SPIO@PSS/CDDP/HSA and SPIO@PSS/CDDP/HSA–MTX NPs

The morphologies and particle size of SPIO, SPIO@APTES, SPIO@PSS, SPIO@PSS/CDDP, SPIO@PSS/CDDP/HSA, and SPIO@PSS/CDDP/HSA–MTX NPs were observed under TEM (Hitachi H-7500, Tokyo, Japan) with 2% uranyl acetate (UA) staining. The size distribution and zeta potentials of the prepared nanoparticles were evaluated using a Zetasizer Nano-ZS90 (Malvern Instruments Ltd, UK). Moreover, after preparation of SPIO@PSS/CDDP/HSA and SPIO@PSS/CDDP/HSA–MTX and centrifugation at 20,000 g for 10 min, the un-loaded CDDP in the supernatant was detected by using an inductively coupled plasma optical emission spectrometry (Optima 7000 DV ICP-OES Spectrometer, Perkin Elmer, USA). The CDDP encapsulation efficiency, measured in percent, was calculated as

$$EE = (Wf - Wu)/Wf \times 100\%$$

where Wf is the weight of the feeding CDDP, and Wu is the weight of the un-loaded CDDP.

Next, the stability of the particles in different environments was assessed. For this purpose, the centrifuged SPIO@PSS/CDDP/HSA and SPIO@PSS/CDDP/HSA–MTX NPs were resuspended in 1 mL PBS or saline solution at 4°C. Particle size at 0, 1, 3, 6, 10, 14, 21, and 28 days was determined using a Zetasizer Nano-ZS90. Moreover, the stability of the particles in the Dulbecco's Modified Eagle Medium (DMEM) supplemented with 10% (v/v) FBS at 4°C was also evaluated at 0, 1, and 3 days using a Zetasizer Nano-ZS90.

In vitro Heat Generation Measurement

A radiofrequency generator (RF, Power-cube 32 High Frequency Induction System; President Honor Industries Co., New Taipei City, Taiwan) with 2.24 kW of power and a frequency of 1300–1800 Hz using a sine wave was used to expose to various aqueous solutions for 30 min: double-distilled water (ddH_2O), Roswell Park Memorial Institute (RPMI) 1640 culture medium, SPIO@APTES, SPIO@PSS/CDDP/HSA, and SPIO@PSS/CDDP/HSA–MTX. A coil of inner diameter 10 mm formed from a conductive copper wire with a diameter 2 mm was served as the RF induction antenna and actively water-cooled using an automatic pumping system. The samples were placed immediately under the center of the coil, and the change in temperature of the particle solution was recorded every 10 s using an infrared thermal imaging camera (Thermo Shot F30, Nippon Avionics Co., Ltd., Japan) to evaluate the rate of temperature increase. Following RF exposure, we next characterized changes in particle distribution and morphology of the SPIO@PSS/CDDP/HSA and SPIO@PSS/CDDP/HSA–MTX NPs using a Zetasizer Nano-ZS90 and TEM.

In vitro Cytotoxicity and Cellular Uptake of the Prepared Nanoparticles

A human lung large cell carcinoma cell line (NCI-H661) and a pulmonary adenocarcinoma cell line (A549) were acquired from Bioresource Collection and Research Center

(BCRC, Taiwan) and used to perform the cell viability studies. A549 and NCI-H661 cells were maintained separately in RPMI-1640 medium supplemented with 10% (v/v) FBS and 1% (v/v) Gibco® antibiotic-antimycotic solution at 37°C under a humidified atmosphere containing 5% CO_2. In vitro cytotoxicity was evaluated using an MTT assay. NCI-H661 or A549 cells were separately incubated on 48-well plates at a density of 2×10^6 cells/well for 24 h. Then, the culture media was replaced with fresh media containing CDDP, SPIO@PSS/HSA, SPIO@PSS/CDDP/HSA, SPIO@PSS/HSA−MTX, or SPIO@PSS/CDDP/HSA−MTX at respective CDDP concentrations of 0, 0.1, 1, 10, and 100 μM. After 48 h, the cells were cultured in fresh medium containing MTT reagents and incubated for another 3 h. Finally, the absorbance was measured at 570 nm by a UV-vis spectrophotometer/microplate reader (SpectraMax Plus, Molecular Devices, USA).

The glass plate was seeded with NCI-H661 or A549 cells and placed in a Petri dish overnight, and then covered with fresh medium containing the FITC-modified SPIO@PSS/CDDP/HSA and SPIO@PSS/CDDP/HSA−MTX NPs. In order to determine the effects of active targeting and receptor-mediated endocytosis by MTX-conjugation, the cells were pre-treated with 2 mM folic acid for 1 h and then fed with FITC-modified SPIO@PSS/CDDP/HSA−MTX NPs. After incubation for 24 h, the glass plate was washed twice with PBS to remove the un-uptake nanoparticles before the cells were fixed with 10% formalin and then observed under a spectral confocal multiphoton system (Leica TCS SP8, Wetzlar, Germany). The average fluorescent intensity of FITC in cells was quantified with Leica Application Suite X software (Leica Microsystems Inc., Illinois, USA) to demonstrate the content of nanoparticle uptake. Each result represented an average of five randomized regions of each sample, and the brightness of the SPIO@PSS/CDDP/HSA NP-treated group was designated as 100% for each individual lung cancer cell line.

Furthermore, Fe content in cells was determined by Prussian blue reaction.[39] Briefly, the NCI-H661 or A549 cells were cultured on 24-well plates, at a density of 1×10^5 cells/well, for 24 h and then treated with SPIO@PSS/CDDP/HSA or SPIO@PSS/CDDP/HSA−MTX for 24 h. At the same time, the cells were pre-treated with 2 mM folic acid for 1 h after which SPIO@PSS/CDDP/HSA−MTX NPs were fed for 24 h. The cells were washed twice with PBS, fixed with 10% paraformaldehyde solution for 5 min, and immersed in a $K_4[Fe(CN)_6]\cdot 3H_2O$/HCl mixture (equal volumes of 10% potassium ferrocyanide and 20% HCl aqueous solution) for 20 min to form a bright blue pigment (ferric ferrocyanide). The plates were then observed under an Olympus IX 71 inverted microscope (U-DCD, Olympus Corporation, Tokyo, Japan) to determine the Fe content in cells. Moreover, the cellular uptake of nanoparticles by optical dark-field reflectance images could be simultaneously captured using an Olympus IX 71 inverted microscope with a dark-field condenser.[40]

In vitro Cytotoxicity of the Combination of Chemotherapy with Hyperthermia

To determine the synergistic effect of the combined chemotherapy with hyperthermia, the NCI-H661 or A549 cells were seeded into a 48-well plate (2×10^5 cells/well) and incubated for 24 h. The cells were treated with SPIO@PSS/HSA−MTX or SPIO@PSS/CDDP/HSA−MTX at a CDDP concentration of 0, 0.1, 1, 10, or 100 μM. After the 24 h incubation, the cells were collected in Eppendorf tubes and exposed to RF at 2.24 kW of power and a frequency of 1300–1800 Hz using a sine wave for 5, 10, 20, or 30 min. The cells were then re-cultured in 48-well plates for another 24 h and then subjected to the MTT assay.

In vivo Antitumor Efficacy

Female BALB/cAnN.Cg-Foxnlnu/CrlNarl nude mice with 4-week age purchased from the National Laboratory Animal Center (Taipei, Taiwan) were subcutaneously injected into the right flank region with a 100-μL PBS solution containing 1×10^7 A549 cells to develop the A549 xenograft tumor mouse model. The tumor size was measured every 2 days, and tumor volume was calculated according to the formula as $1/2 \times a \times b^2$, where a is the length and b is the width of the tumor.

When the tumor volume reached 100–150 mm^3, five groups of tumor-bearing mice (n = 5 in each group) were, respectively, treated with (a) saline, (b) free CDDP (5 mg of CDDP/kg),[41] (c) SPIO@PSS/CDDP/HSA−MTX NPs (5 mg of CDDP/kg, 58 mg of SPIO@APTES/kg), (d) SPIO@PSS/HSA−MTX (58 mg of SPIO@APTES/kg) with RF exposure, or (e) SPIO@PSS/CDDP/HSA−MTX NPs (5 mg of CDDP/kg, 58 mg of SPIO@APTES/kg) with RF exposure. For the RF-treated groups, the xenograft tumor was exposed for 30 min using an RF generator with 2.24 kW of power and a frequency of 1300–1800 Hz

using a sine wave 24 h after injection. The mice received only once intravenous injection at day 0, and the tumor sizes and the body weights were recorded every 2 days for 24 days. Moreover, the tumors and main tissues (heart, liver, spleen, lung, and kidneys) in each group were excised and fixed in 10% paraformaldehyde solution at the 24th day of treatment for histopathological tests. Herein, all experimental mice received care according to the guidelines outlined in the Guide for the Care and Use of Laboratory Animals (8th edition), and animal experiments were performed according to the protocols approved by the National Taiwan University College of Medicine and College of Public Health Institutional Animal Care and Use Committee.

Statistical Analysis

All experimental data were expressed as mean ± standard deviation. Statistical significance between groups was determined by Student's *t*-test. A *p*-value less than 0.05 was accepted as statistically significant.

Results and Discussion

Characterization of the MTX−HSA Conjugate

In a previous study, we have successfully conjugated chitosan with folic acid via EDC as a carboxyl activating agent.[14] Herein, the synthesis of MTX−HSA conjugate was performed by chemically linking MTX to HSA via EDC at the selected MTX:HSA molar ratio of 2. FT-IR spectra of the HSA, MTX−HSA conjugate, and pure MTX are shown in Figure 1A. The characteristic FT-IR absorption peak of MTX at 1100 cm^{-1} was observed in the spectrum of MTX−HSA conjugate and assigned to the C–N bond.[42] The most significant IR frequencies of the HSA and MTX−HSA conjugate were the amide I band and the amide II band, representing the C=O stretching and N−H deformation, respectively. The FT-IR absorption peak of the amide I band typically appears around 1720 −1740 cm^{-1} and is moved to lower frequencies after hydrogen bonding formation. The amide II band typically appears between 1500 and 1560 cm^{-1} and is shifted to higher frequencies when hydrogen-bond is formed.[43] As shown in Figure 1A, the peak at 1631 cm^{-1} represents bonded C=O stretching, while the peak at about 1716 cm^{-1} represents free C=O stretching. A relatively high frequency at 1563 cm^{-1} indicates the amide II band with hydrogen-bond. The peaks at about 1536 and 1556 cm^{-1} belong to free N−H bending.[14] Table 1 shows that the intensity ratio of amide II/I increased with MTX conjugation, indicating successful conjugation of MTX with HSA.

The UV-vis absorption spectra of HSA, MTX−HSA conjugate, and MTX are shown in Figure 1B. The UV spectra of MTX and MTX−HSA conjugate showed an absorption maximum at 375 nm, whereas HSA alone showed no such maximum. These results clearly indicate the formation of a conjugate of MTX with HSA. Moreover, the MTX:HSA molar ratio of 1.22 in MTX −HSA conjugate, estimated from the intensity of the absorption maximum (375 nm) of MTX derivative in MTX−HSA conjugate, was lower than the selected MTX:HSA molar ratio of 2. The yield of MTX−HSA conjugate in this modification process was about 80%.

Characterization of SPIO@PSS/CDDP/HSA and SPIO@PSS/CDDP/HSA−MTX NPs

SPIO@PSS/CDDP/HSA and SPIO@PSS/CDDP/HSA −MTX NPs were formulated by using the LbL coating method. Figure 2 and Table 2 show the size distribution, average particle size, and zeta potential of SPIO@PSS, SPIO@PSS/CDDP, SPIO@PSS/CDDP/HSA, and SPIO@PSS/CDDP/HSA−MTX NPs. Particle size after addition of PSS to the SPIO@(3-aminopropyl)triethoxysilane (APTES) solution to form SPIO@PSS NPs was much greater (125.9 nm) than that of SPIO@APTES (25.1 nm). TEM analysis revealed that SPIO@APTES NPs were distributed in the PSS polymer matrix, indicating that positively charged SPIO@APTES NPs self-assembled with PSS polymers to form a nano-complex (Figure 2C). The average size and zeta potential of SPIO@PSS/CDDP NPs was 125.8 nm and −40.4 mV, respectively. The difference in surface charge between SPIO@PSS and SPIO@PSS/CDDP NPs indicates that the coating of SPIO@PSS with CDDP molecules was successful. After coating with HSA, SPIO@PSS/CDDP/HSA exhibited a particle size of 189.8 nm with a zeta potential of 6.4 mV at pH 4.2. For SPIO@PSS/CDDP NPs coated with HSA−MTX, particle size was 192.1 nm, with a positive surface charge (zeta potential of 7.4 mV) at pH 4.2. At pH 7.4, above the isoelectric point of HSA (pI 4.7),[44] the surface particle charge changed from positive to negative either for SPIO@PSS/CDDP/HSA or SPIO@PSS/CDDP/HSA-MTX NPs (Figure 2B). Therefore, the increase in particle size and the change in zeta potential display that the LbL coating of SPIO@PSS with CDDP and HSA or

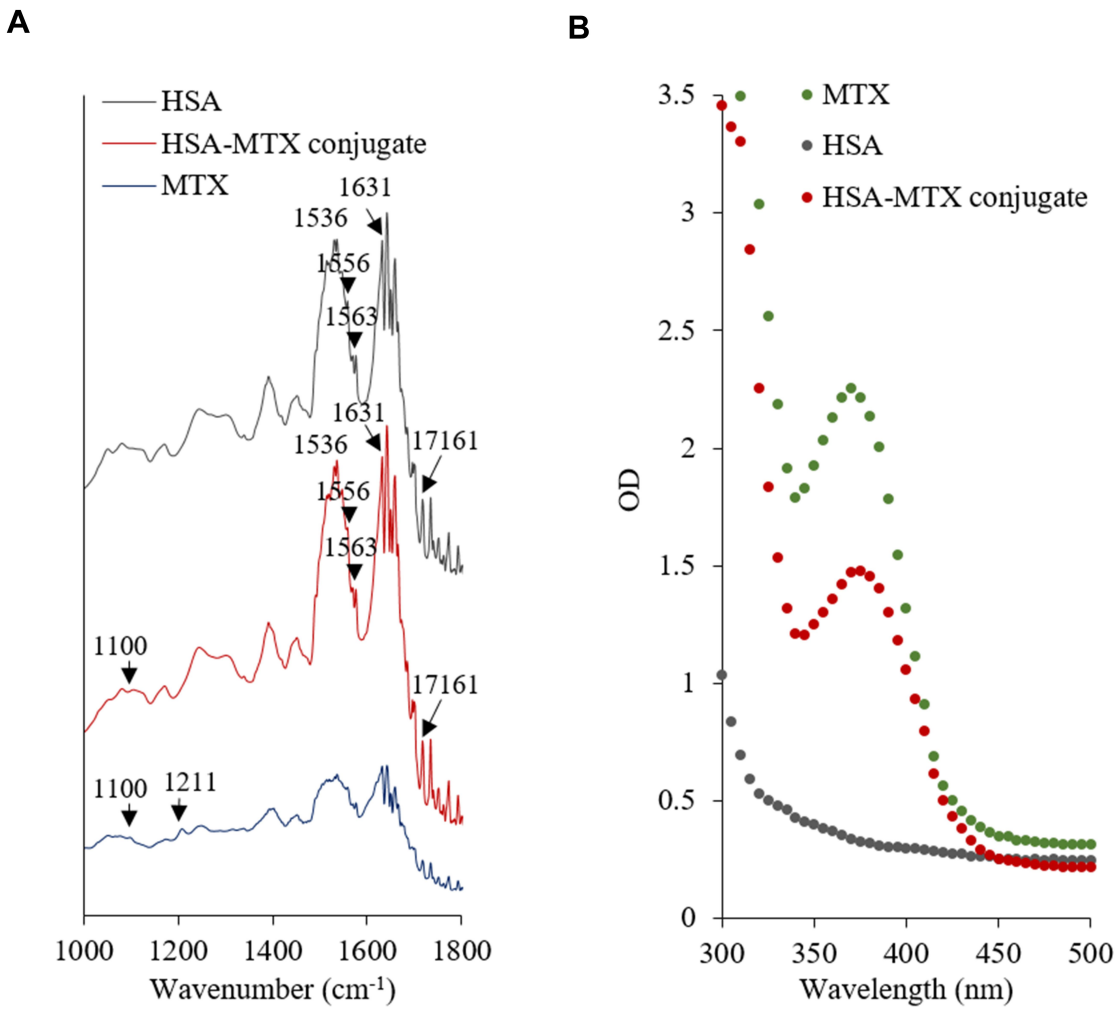

Figure 1 (**A**) FT-IR spectra and (**B**) UV-vis spectra of HSA, MTX, and HSA–MTX conjugates.

HSA−MTX was successful. Moreover, CDDP was well incorporated into nanoparticles, with a loading efficiency of 35.8% for SPIO@PSS/CDDP/HSA and 35.4% for SPIO@PSS/CDDP/HSA−MTX (Table 2).

Ideally, pharmaceutical preparations have good stability for a certain period of preservation to be easily used in a real-world clinic. Therefore, the colloidal stabilities of SPIO@PSS/CDDP/HSA and SPIO@PSS/CDDP/HSA −MTX NPs in phosphate buffer solution (PBS) or saline were assessed by means of a storage period of 4 weeks at 4° C. As shown in Figure 3A, particle size in PBS solution decreased slightly with increasing incubation time for both SPIO@PSS/CDDP/HSA and SPIO@PSS/CDDP/HSA −MTX NPs. Meanwhile, in saline no significant change in particle size was found for SPIO@PSS/CDDP/HSA or SPIO@PSS/CDDP/HSA−MTX NPs (Figure 3B), indicating excellent stability in saline and demonstrating that the nanoparticle solution could be preserved in saline for 4 weeks before use. Furthermore, the stability of SPIO@PSS/CDDP/HSA or SPIO@PSS/CDDP/HSA−MTX NPs in culture medium with 10% FBS supplement was good without aggregation for over 3 days, demonstrating that the HSA- or HSA−MTX-coated NPs could protect from undesired protein absorption and severe aggregation in the blood during circulation (Figure 3C).[45]

In vitro Heat Generation Measurement

To evaluate the potential use of the designed nanoparticle as a hyperthermia inducer, an RF generator at a power of 2.24 kW was applied to expose to ddH_2O, RPMI-1640 culture medium, SPIO@APTES, SPIO@PSS/CDDP/HSA, and SPIO@PSS/CDDP/HSA−MTX NP aqueous solutions for 30 min, with temperature changes recorded every 10 s by an infrared thermal imaging camera. As shown in Figure 4A, the temperature increase rates of the SPIO@PSS/CDDP/HSA and SPIO@PSS/CDDP/HSA

Table 1 Relative Intensity Ratio of N—H Bending Vs C=O Stretching in HSA and HSA–MTX Conjugate

Sample	Band		Wavenumber (cm^{-1})	Intensity Ratio (Amine II/Amine I)
HSA	Amine II	Free N-H	1536 1556	1.505
		Bonded N-H	1563	
	Amine I	Bonded C=O	1631	1
		Free C=O	1716	
HSA−MTX conjugate	Amine II	Free N-H	1536 1556	1.539
		Bonded N-H	1563	
	Amine I	Bonded C=O	1631	1
		Free C=O	1716	

−MTX NP solutions were much higher than that of the SPIO@APTES NPs solution for a given SPIO@APTES concentration of 0.622 mg/mL, indicating that the SPIO@PSS/CDDP/HSA and SPIO@PSS/CDDP/HSA −MTX NPs were much more effective for hyperemia. Previous studies have revealed that the dispersed magnetic nanoparticles with small size are not able to effectively heat in electromagnetic fields, but the sufficient nanoparticle heating can be achieved if they are appropriately aggregated in a space.[46,47] Therefore, trapping of SPIO@APTES NPs in the SPIO@PSS/CDDP/HSA and SPIO@PSS/CDDP/HSA−MTX NPs may have shortened the distance between magnetic nanoparticles to facilitate easier heating under RF treatment.

To detect changes in the prepared nanoparticles after RF irradiation, we performed DLS measurement on both RF-irradiated and control samples. The results for size distribution of SPIO@PSS/CDDP/HSA and SPIO@PSS/CDDP/HSA−MTX NPs with or without RF irradiation are reported in Figure 4B, revealing no significant difference in average size associated with RF irradiation, while the standard deviation of size grew with RF irradiation by 50.6% for SPIO@PSS/CDDP/HSA and by 76.4% for SPIO@PSS/CDDP/HSA−MTX NPs. These results indicate the existence of a morphological effect induced on the prepared nanoparticles by RF irradiation. Compared to the TEM image of SPIO@PSS/CDDP/HSA NPs shown in Figure 2C, the RF-irradiated SPIO@PSS/CDDP/HSA NPs were characterized by the presence of aggregation, with more SPIO@APTES nanoparticles condensed at the center (Figure 4C). In addition, SPIO@PSS/CDDP/HSA and SPIO@PSS/CDDP/HSA−MTX NPs treated with RF irradiation appeared as aggregates of thick-short strips. These results suggest that RF irradiation induced morphological change in the prepared nanoparticles.

In vitro Cytotoxicity and Cellular Uptake of Prepared Nanoparticles

We used the MTT assay to estimate in vitro cytotoxicity of SPIO@PSS/HSA, SPIO@PSS/CDDP/HSA, SPIO@PSS/HSA−MTX, and SPIO@PSS/CDDP/HSA−MTX NPs compared to that of CDDP in two lung cancer cell lines: a human lung large cell carcinoma cell line (NCI-H661) and a pulmonary adenocarcinoma cell line (A549). As shown in Figure 5A, both SPIO@PSS/CDDP/HSA−MTX NPs and CDDP exhibited the dose-dependent cytotoxicity in lung cancer cells. The viability of A549 cells treated with SPIO@PSS/CDDP/HSA−MTX NPs was similar to that of cells treated with free CDDP at equivalent CDDP concentrations of 0.1, 1, and 10 μM. However, the SPIO@PSS/CDDP/HSA−MTX NPs with a 100 μM CDDP concentration displayed a higher cytotoxicity on A549 cells than free CDDP. The viability of the NCI-H661 cells treated with SPIO@PSS/CDDP/HSA or SPIO@PSS/CDDP/HSA−MTX NPs was higher than that of cells treated with CDDP, especially at high CDDP doses (10 and 100 μM). Moreover, viability was higher than 90% for NCI-H661 and A549 cells treated with the prepared nanoparticles without CDDP loading, namely SPIO@PSS/HSA and SPIO@PSS/HSA−MTX NPs. These results indicate that the designed nanocarrier has high biocompatibility, and the cytotoxicity comes directly from the toxicity of loaded CDDP rather than conjugated MTX, even though MTX is a member of the class of antifolate therapeutic agents used in cancer treatment. The half maximal inhibitory concentrations (IC_{50}) of

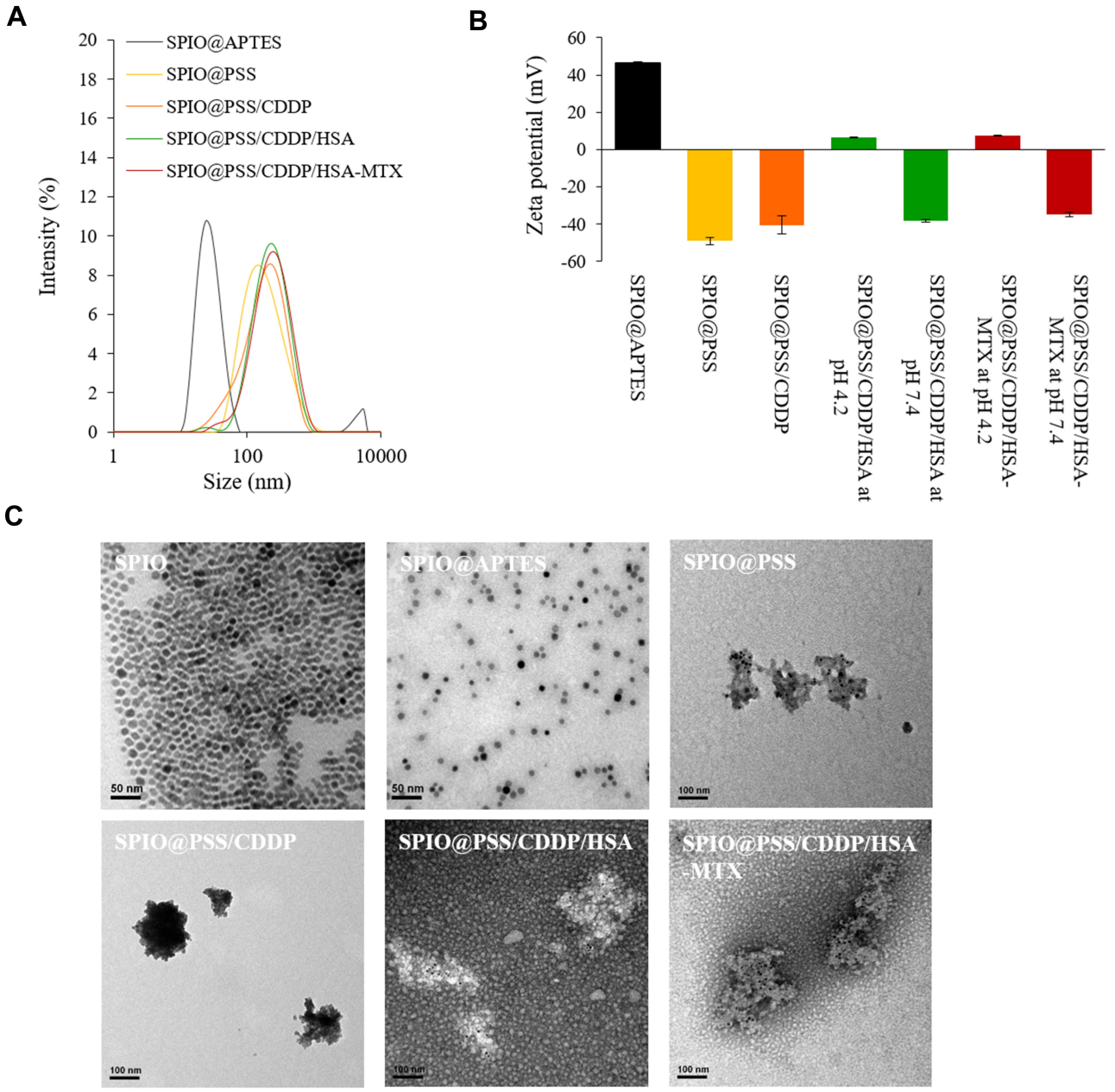

Figure 2 (**A**) The size distribution of nanoparticles after layer-by-layer coating with PSS, CDDP, and HSA or HSA–MTX conjugates. (**B**) The zeta potential of nanoparticles after layer-by-layer coating with PSS, CDDP, and HSA or HSA–MTX conjugates. (**C**) Transmission electron microscopy (TEM) images of SPIO, SPIO@APTES, SPIO@PSS, SPIO@PSS/CDDP, SPIO@PSS/CDDP/HSA, and SPIO@PSS/CDDP/HSA–MTX nanoparticles. Samples were negatively stained with 2% uranyl acetate (UA) before imaging. Scale bar=100 nm.

CDDP, SPIO@PSS/CDDP/HSA, and SPIO@PSS/CDDP/HSA−MTX NPs toward NCI-H661 cells were 29.3, 191.6, and 545.6 μM, respectively. The IC_{50} of CDDP for A549 cells was 75.6 μM, whereas that of SPIO@PSS/CDDP/HSA−MTX NPs was 47.8 μM, 1.6 times as cytotoxic as CDDP.

Figure 5B shows the fluorescence of FITC observed under a spectral confocal multiphoton system in NCI-H661 and A549 cells, which were fed with FITC-modified SPIO@PSS/CDDP/HSA or SPIO@PSS/CDDP/HSA−MTX for 24 h. The green brightness of FITC increased in the MTX-modified nanoparticles in both NCI-H661 and A549 cells (Figure 5B). As determined by Prussian blue-staining, the iron content in cells with SPIO@PSS/CDDP/HSA−MTX NPs treatment was higher than in cells with SPIO@PSS/CDDP/HSA NPs treatment. The scattered white color of magnetic nanoparticle probes under a dark-field microscope has been applied previously

Table 2 Particle Size and Loading Efficiency of CDDP in the Prepared Nanoparticles

Sample	Size (nm)	PdI	LD (%)
SPIO@PSS	125.9 ± 15.60	0.335	—
SPIO@PSS/CDDP	125.8 ± 15.79	0.367	—
SPIO@PSS/CDDP/HSA	189.8 ± 4.75	0.266	35.8 ± 0.86
SPIO@PSS/CDDP/HSA −MTX	192.1 ± 3.10	0.280	35.4 ± 0.87

in biosensing applications.[48] Herein, the magnetic nanoparticles captured in the designed SPIO@PSS/CDDP/HSA or SPIO@PSS/CDDP/HSA−MTX NPs and fed to lung cancer cells were visualized under dark-field microscopy. As shown in Figure 5B, individual cells treated with SPIO@PSS/CDDP/HSA−MTX NPs exhibited stronger white light than individual cells treated with SPIO@PSS/CDDP/HAS. Moreover, when cells were pre-treated with 2 mM free folic acid for 1 h and then fed with SPIO@PSS/CDDP/HSA−MTX, there were no significant differences between SPIO@PSS/CDDP/HSA and SPIO@PSS/CDDP/HSA−MTX groups in terms of FITC-fluorescence, Prussian blue-staining, or dark-field imaging. This finding suggests that free folic acid molecules competed with SPIO@PSS/CDDP/HSA−MTX for folate receptors, suppressing the receptor-mediated endocytosis of particles. These results demonstrate that MTX−HSA conjugate substantially enhanced the cell uptake and accumulation of SPIO@PSS/CDDP/HSA−MTX NPs in NCI-H661 and A549 cells by folate receptor-mediated endocytosis.

As presented in Figure 5C, A549 cells fed with MTX-conjugated nanoparticles (SPIO@PSS/CDDP/HSA−MTX NPs) exhibited substantial FITC fluorescent intensity in comparison with NCI-H661 cells. This difference might be due to the more expression of folate receptor in A549 cells,[49] resulting in high effect for folate receptor-mediated endocytosis in A549 cells compared with that in NCI-H661 cells. These results also demonstrate that enhancements in cellular association, uptake, and cytotoxicity

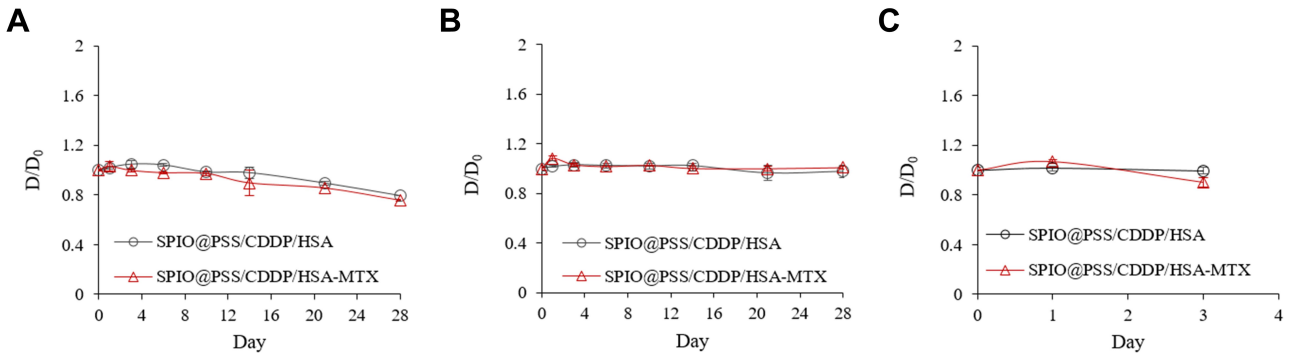

Figure 3 Stability of SPIO@PSS/CDDP/HSA and SPIO@PSS/CDDP/HSA–MTX nanoparticles, as revealed by relative diameter change compared to the particle size at Day 0 (D/D_0) in (**A**) PBS, (**B**) saline, and (**C**) DMEM supplemented with 10% FBS.

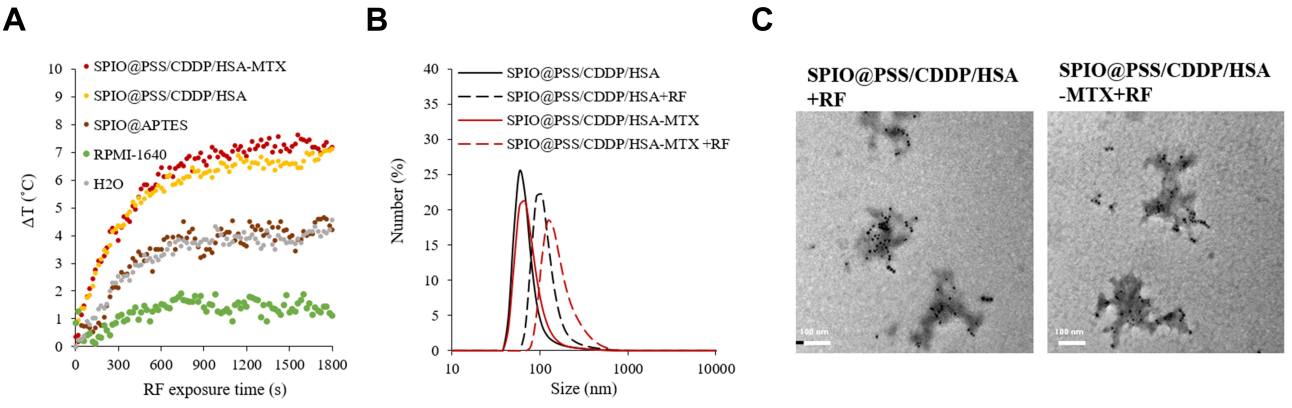

Figure 4 (**A**) Heating curves for H_2O, PRMI-1640 medium, SPIO@APTES, SPIO@PSS/CDDP/HSA, and SPIO@PSS/CDDP/HSA–MTX nanoparticles. The concentration of SPIO@APTES was 0.622 mg/mL. (**B**) Number-based particle size distribution of SPIO@PSS/CDDP/HSA and SPIO@PSS/CDDP/HSA−MTX nanoparticles with or without RF exposure. (**C**) TEM images showing that RF irradiation affected the morphology of SPIO@PSS/CDDP/HSA and SPIO@PSS/CDDP/HSA−MTX nanoparticles. Scale bar=200 nm.

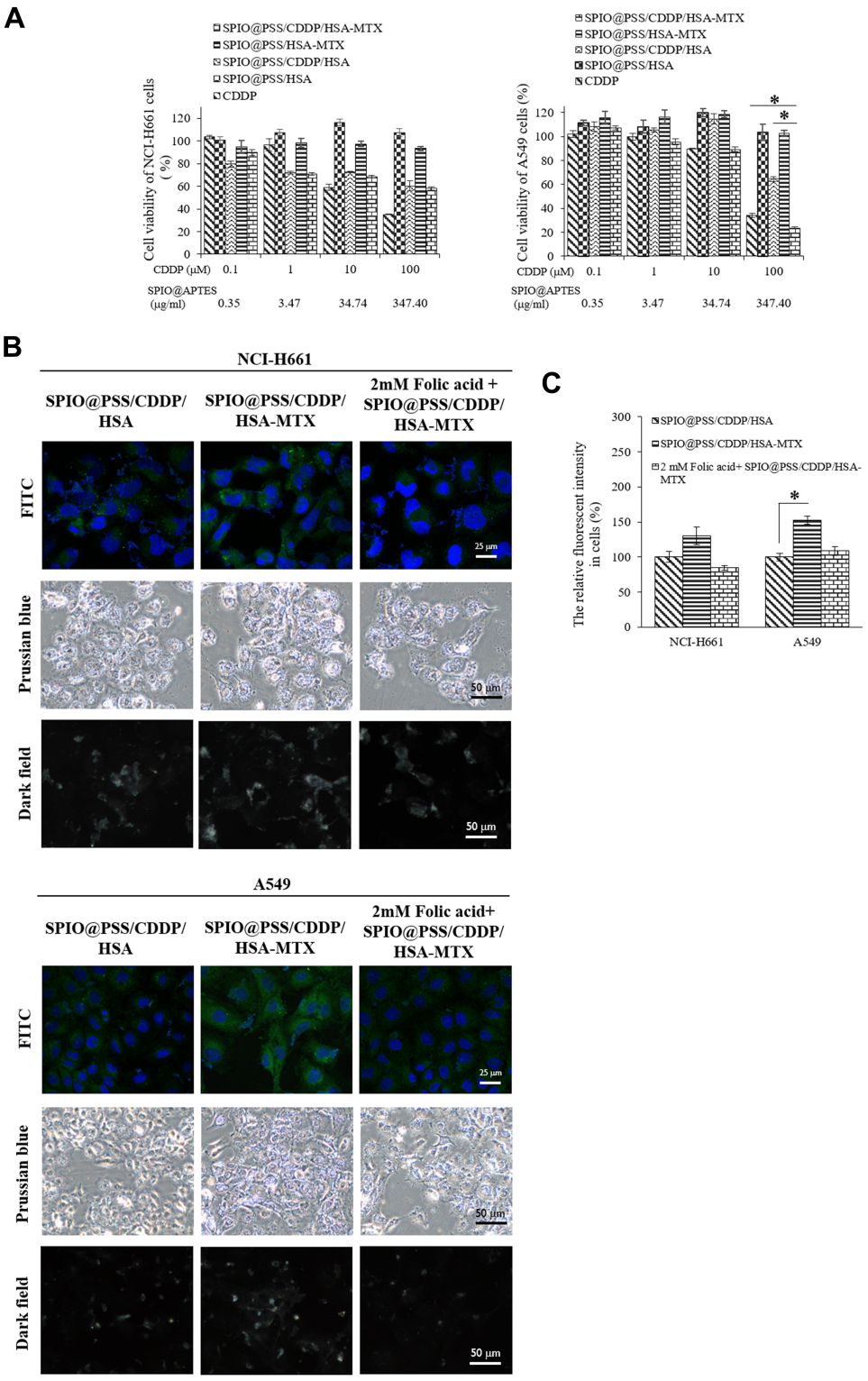

Figure 5 (**A**) The viability of NCI-H661 and A549 cells after treatment with CDDP, SPIO@PSS/HSA, SPIO@PSS/CDDP/HSA, SPIO@PSS/HSA–MTX, and SPIO@PSS/CDDP/HSA–MTX nanoparticles for 48 h. (**B**) Cellular uptake of SPIO@PSS/CDDP/HSA and SPIO@PSS/CDDP/HSA–MTX nanoparticles in NCI-H661 and A549 cells with or without 2 mM folic acid pre-treatment. (**C**) Relative fluorescent intensity of FITC in NCI-H661 and A549 cells, with * indicating $p < 0.05$.

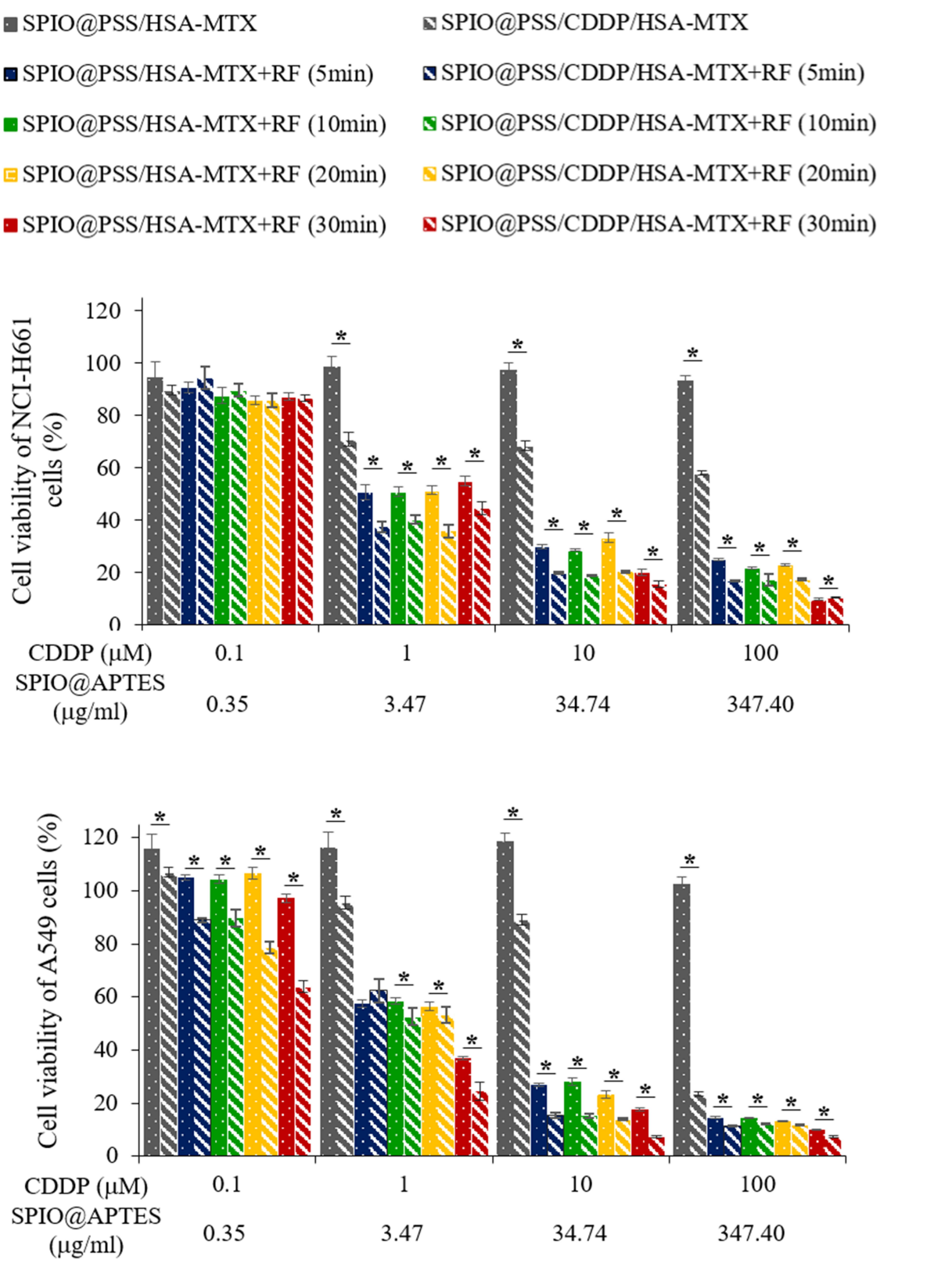

Figure 6 Viability of NCI-H661 and A549 cells treated with SPIO@PSS/HSA–MTX and SPIO@PSS/CDDP/HSA–MTX at various CDDP concentrations and RF (2.24 kW) exposure periods. * indicates $p < 0.05$.

were induced by the specific interaction of MTX-conjugated nanoparticles with their receptor and by subsequent internalization through receptor-mediated endocytosis.

In vitro Cytotoxicity of the Combination of Chemotherapy with Hyperthermia

To investigate the in vitro synergic effect of combined chemotherapy and hyperthermia, an MTT assay was used to determine the viabilities of NCI-H661 and A549 cells after treatment with SPIO@PSS/HSA−MTX or SPIO@PSS/CDDP/HSA−MTX NPs with RF irradiation for 0, 5, 10, 20, or 30 min. As shown in Figure 6, SPIO@PSS/HSA−MTX NPs with various RF irradiation periods exhibited slight cytotoxicity to the NCI-H661 and A549 cells at a SPIO@APTES concentration of 0.35 μg/mL but displayed serious cell injury at SPIO@APTES concentrations of 3.47, 34.74, and 347.40 μg/mL. This behavior suggests that hyperthermia could be used to directly kill cancer cells and might increase the sensitivity of cancer cells to the toxicity of low-dose MTX. However, when A549 cells with SPIO@PSS/CDDP/HSA−MTX NPs pre-treatment were RF-irradiated, significant cytotoxicity was observed compared with that of A549 cells treated with SPIO@PSS/HSA−MTX NPs and RF irradiation, with cell viability showing CDDP dose-dependence. Moreover, for A549 cells treated with SPIO@PSS/CDDP/HSA−MTX NPs at CDDP concentrations of 1, 10, and 100 μM, cytotoxicity showed dependence on the RF irradiation period. These results indicate that hyperthermia not only could be used to directly kill tumor cells but also could effectively increase the sensitivity of cancer cells to chemotherapy.[18,19] A549 cells treated with a combination of chemotherapy and hyperthermia displayed a stronger antitumor effect than NCI-H661 cells. This finding indicates that the effect of MTX conjugation on SPIO@PSS/CDDP/HSA NPs (SPIO@PSS/CDDP/HSA−MTX) not only increases the uptake of nanoparticles in folate receptor-expressing cells

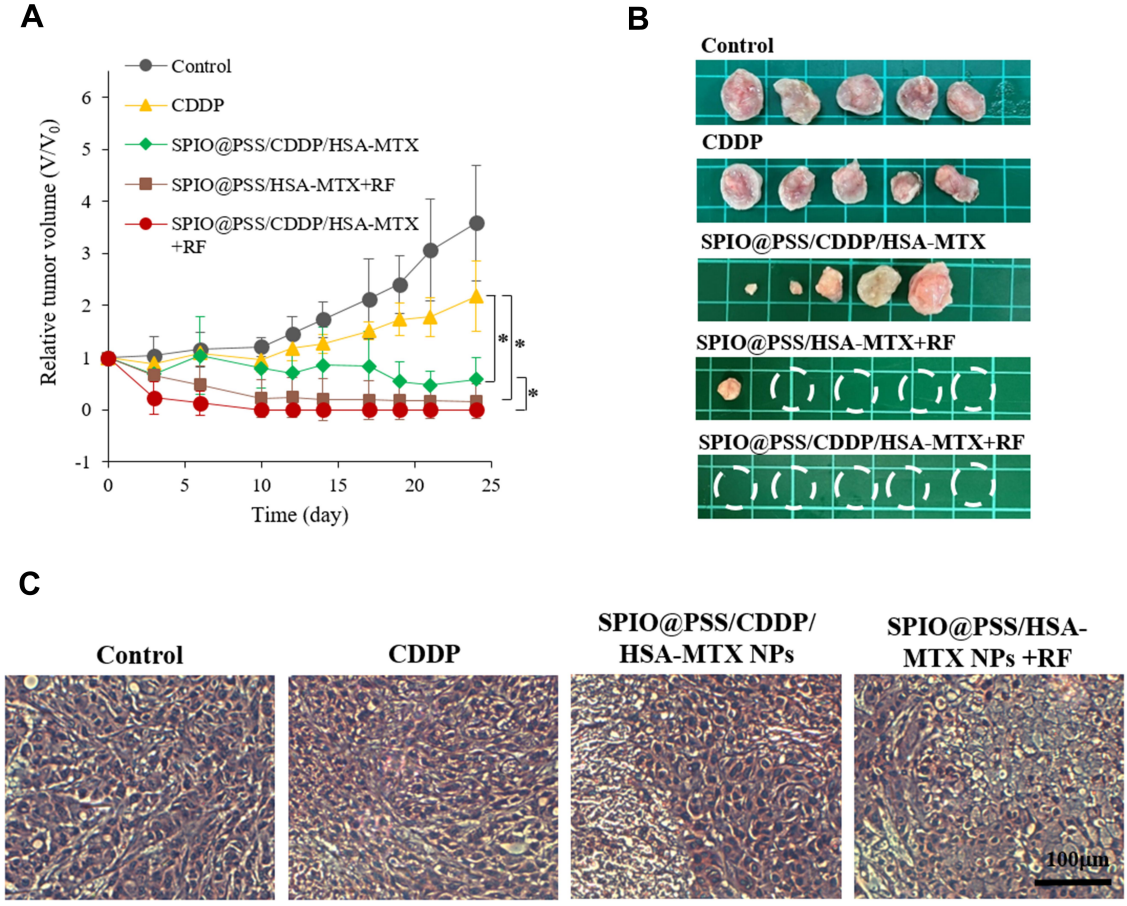

Figure 7 (**A**) Relative tumor volume, (**B**) representative tumor images, and (**C**) H&E-stained images of tumor tissue treated with saline, free CDDP, SPIO@PSS/CDDP/HSA–MTX, SPIO@PSS/HSA–MTX, or SPIO@PSS/CDDP/HSA–MTX with RF generator irradiation (2.24 kW, 30 minutes) at 24 days. Scale bar=100 μm. * indicates $p < 0.05$.

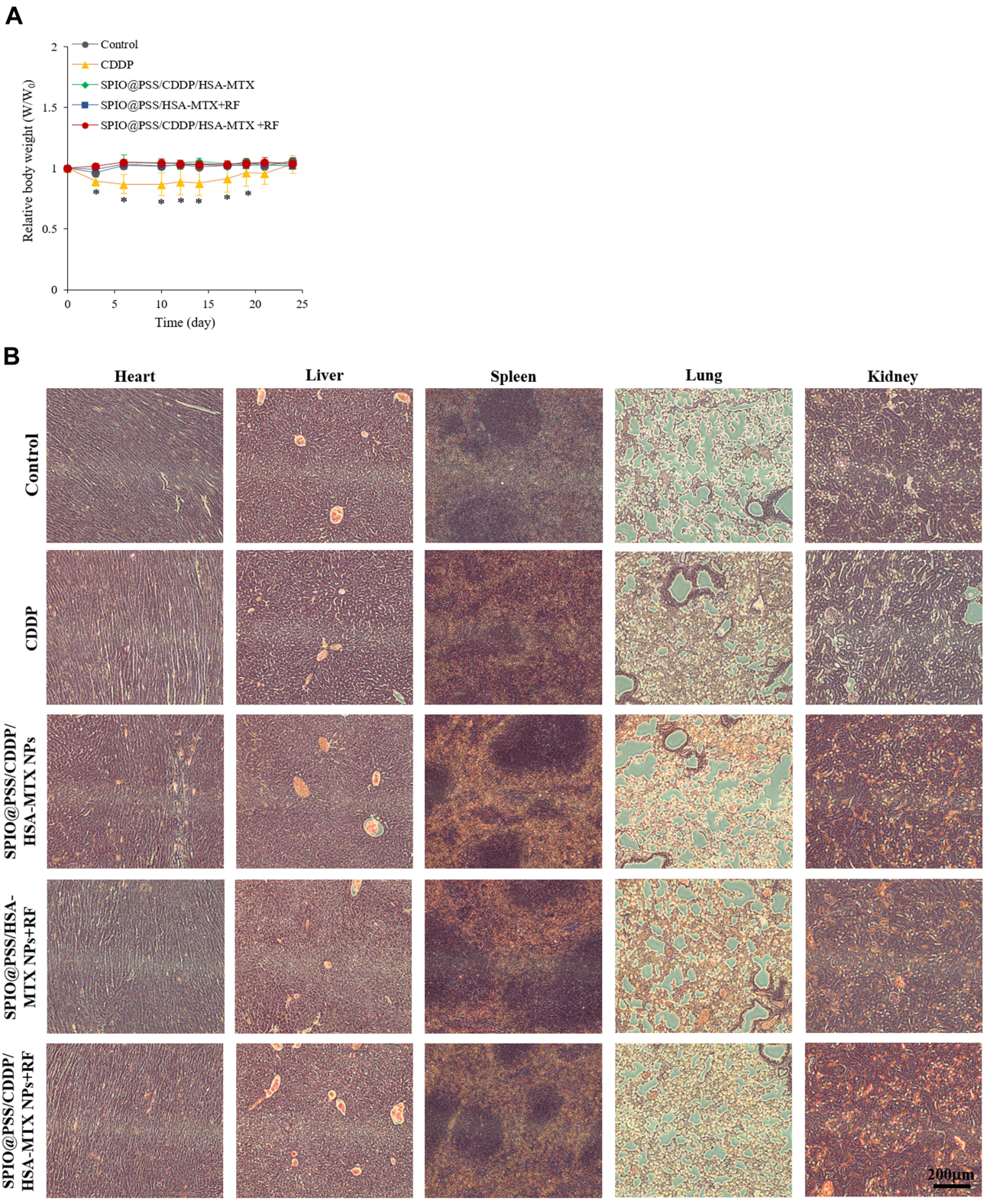

Figure 8 (**A**) Relative body weights of nude mice and (**B**) H&E-stained images of heart, liver, spleen, lung, and kidney tissue in mice after treatment with saline, free CDDP, SPIO@PSS/CDDP/HSA–MTX, SPIO@PSS/HSA–MTX, or SPIO@PSS/CDDP/HSA–MTX with RF generator irradiation (2.24 kW, 30 minutes) at 24 days. Scale bar=200 μm. * indicates $p < 0.05$.

(A549 cells) but also improves the elimination of folate receptor-expressing cells after hyperthermia treatment.

In vivo Antitumor Efficacy

Therapeutic effect was assessed by examining tumor volumes of mice intravenously pre-injected with saline, free CDDP, SPIO@PSS/CDDP/HSA−MTX NPs with RF irradiation, and SPIO@PSS/CDDP/HSA−MTX NPs without RF irradiation. Groups with SPIO@PSS/HSA−MTX NPs and RF treatments were used to evaluate the hyperthermia effect on tumor growth. The mice were intravenously injected only once at day 0, and tumor size was normalized to tumor size at day 0. As shown in Figure 7A, the dramatic increases in tumor volume were observed for the groups treated with saline and free CDDP within 24 days. In comparison, the group treated with SPIO@PSS/CDDP/HSA−MTX NPs showed an effective inhibition ability for tumor growth, which could be attributed to effective targeting and accumulation of SPIO@PSS/CDDP/HSA−MTX NPs in the tumor. However, no tumor tissue could be detected in the group treated with SPIO@PSS/CDDP/HSA−MTX NPs followed by RF irradiation, even after 24 more days of observation, indicating a good anticancer effect. Notably, SPIO@PSS/HSA−MTX NP treatment followed by RF irradiation also showed inhibition of tumor growth and elimination of tumor tissues, with a tumor clearance rate of 80%. The actual tumor sizes after different treatments were also recorded by taking photographs of excised tumor tissues (Figure 7B). Hematoxylin-eosin (H&E) staining analysis of tumor tissue was performed and showed in Figure 7C. Compared to the control and free CDDP-treated groups, the groups treated with SPIO@PSS/CDDP/HSA−MTX NPs exhibited more necrosis areas, especially for mice treated with SPIO@PSS/HSA−MTX NPs followed by RF irradiation. These results indicate that SPIO@PSS/CDDP/HSA−MTX NPs, with or without RF irradiation, suppress tumor cell proliferation and enhance anticancer efficacy.

Cisplatin treatment produces anticancer effects coupled with nephrotoxicity, hepatotoxicity, cardiotoxicity, and impaired general health status.[4] The change in body weight is also a main prognostic factor that is associated with survival and a response to treatment.[50] Significant loss of body weight was detected only for the administration of free CDDP and not for any other group at any time within the whole experimental period (Figure 8A). In addition, no pathological signs were observed in H&E histological examinations of the vital organs (heart, liver, spleen, lung, and kidney) (Figure 8B), indicating that none of these treatments would lead to noticeable side effects in these main organs. Treatment using SPIO@PSS/CDDP/HSA−MTX NPs and RF irradiation allows the CDDP-based chemotherapeutic drug to act synergistically with hyperthermia to provide a profound anticancer effect.

Conclusion

In this study, SPIO@PSS/CDDP/HSA−MTX NPs were successfully developed by LbL-coating CDDP and MTX−HSA conjugate onto a SPIO-PSS complex core for lung cancer-specific targeting. Characteristic analysis showed the excellent stability of SPIO@PSS/CDDP/HSA−MTX NPs in saline solution and a higher temperature increase rate under RF irradiation than that of SPIO@APTES nanoparticles. Here, the MTX−HSA conjugate coating enhanced the cellular uptake of SPIO@PSS/CDDP/HSA−MTX NPs and improved the combined effect of hyperthermia with chemotherapy on cancer cells with high folate receptor expression. Furthermore, SPIO@PSS/CDDP/HSA−MTX NPs were applied during combined chemotherapy – hyperthermia therapy and exhibited a synergistic anticancer effect superior to the effect of monotherapy. This work presented a successful approach to fabrication of multifunctional nanoparticles. The favorable potential of this approach for chemotherapy and hyperthermia makes it a powerful candidate for future antitumor therapeutic strategies.

Acknowledgments

The authors appreciate the help from the National Taiwan University College of Medicine and the National Taiwan University Hospital. This work was supported by the Ministry of Science and Technology (MOST 106-2314-B-002-015-MY3 and 108-2314-B-002-117-MY3).

Disclosure

Chung-Hao Wang is an employee of Gene'e Tech Co. Ltd. The authors declare no other potential conflicts of interest for this work and no competing financial interest.

References

1. Shi H, Guo J, Li C, Wang Z. A current review of folate receptor alpha as a potential tumor target in non-small-cell lung cancer. *Drug Des Devel Ther*. 2015;9:4989–4996.

2. Lemjabbar-Alaoui H, Hassan OU, Yang YW, et al. Lung cancer: biology and treatment options. *Biochim Biophys Acta*. 2015;1856(2):189–210.
3. Siegel R, DeSantis C, Virgo K, et al. Cancer treatment and survivorship statistics, 2012. *CA Cancer J Clin*. 2012;62(4):220–241. doi:10.3322/caac.21149
4. Dasari S, Tchounwou PB. Cisplatin in cancer therapy: molecular mechanisms of action. *Eur J Pharmacol*. 2014;740:364–378. doi:10.1016/j.ejphar.2014.07.025
5. Aisner J, Abrams J. Cisplatin for small-cell lung cancer. *Semin Oncol*. 1989;16(4 Suppl 6):2–9.
6. Khafaji M, Zamani M, Vossoughi M, et al. Doxorubicin/cisplatin-loaded superparamagnetic nanoparticles as a stimuli-responsive co-delivery system for chemo-photothermal therapy. *Int J Nanomedicine*. 2019;14:8769–8786. doi:10.2147/IJN.S226254
7. Sudha T, Bharali DJ, Yalcin M, et al. Targeted delivery of cisplatin to tumor xenografts via the nanoparticle component of nano-diamino-tetrac. *Nanomedicine (Lond)*. 2017;12(3):195–205. doi:10.2217/nnm-2016-0315
8. Mamot C, Drummond DC, Noble CO, et al. Epidermal growth factor receptor-targeted immunoliposomes significantly enhance the efficacy of multiple anticancer drugs in vivo. *Cancer Res*. 2005;65(4):11631–11638. doi:10.1158/0008-5472.CAN-05-1093
9. Park EK, Kim SY, Lee SB, et al. Folate-conjugated methoxy poly(ethylene glycol)/poly(epsilon-caprolactone) amphiphilic block copolymeric micelles for tumor-targeted drug delivery. *J Control Release*. 2005;109(1–3):158–168. doi:10.1016/j.jconrel.2005.09.039
10. Jang C, Lee JH, Sahu A, et al. The synergistic effect of folate and RGD dual ligand of nanographene oxide on tumor targeting and photothermal therapy in vivo. *Nanoscale*. 2015;7(44):18584–18594. doi:10.1039/C5NR05067G
11. Ferris DP, Lu J, Gothard C, et al. Synthesis of biomolecule-modified mesoporous silica nanoparticles for targeted hydrophobic drug delivery to cancer cells. *Small*. 2011;7(13):1816–1826. doi:10.1002/smll.201002300
12. Nasongkla N, Shuai X, Ai H, et al. cRGD-functionalized polymer micelles for targeted doxorubicin delivery. *Angew Chem Int Ed Engl*. 2004;43(46):6323–6327. doi:10.1002/anie.200460800
13. Goren D, Horowitz AT, Tzemach D, et al. Nuclear delivery of doxorubicin via folate-targeted liposomes with bypass of multidrug-resistance efflux pump. *Clin Cancer Res*. 2000;6(5):1949–1957.
14. Yang SJ, Lin FH, Tsai KC, et al. Folic acid-conjugated chitosan nanoparticles enhanced protoporphyrin IX accumulation in colorectal cancer cells. *Bioconjug Chem*. 2010;21(4):679–689. doi:10.1021/bc9004798
15. Wong PT, Choi SK. Mechanisms and implications of dual-acting methotrexate in folate-targeted nanotherapeutic delivery. *Int J Mol Sci*. 2015;16(1):1772–1790. doi:10.3390/ijms16011772
16. Zwicke GL, Mansoori GA, Jeffery CJ. Targeting of cancer nanotherapeutics. *Nano Rev*. 2012;1:1–11.
17. Simon HB. Hyperthermia. *N Engl J Med*. 1993;329:483–487. doi:10.1056/NEJM199308123290708
18. Tan G, Chia C, Kumar M, et al. 201 consecutive cytoreductive surgery (CRS) and hyperthermic intraperitoneal chemotherapy (HIPEC) procedures in a single Asian tertiary centre. *Int J Hyperthermia*. 2017;33(3):288–294. doi:10.1080/02656736.2016.1262064
19. Datta NR, Krishnan S, Speiser DE, et al. Magnetic nanoparticle-induced hyperthermia with appropriate payloads: paul Ehrlich's "magic (nano)bullet" for cancer theranostics? *Cancer Treat Rev*. 2016;50:217–227. doi:10.1016/j.ctrv.2016.09.016.
20. Veiseh O, Gunn JW, Zhang M. Design and fabrication of magnetic nanoparticles for targeted drug delivery and imaging. *Adv Drug Deliv Rev*. 2010;62(3):284–304. doi:10.1016/j.addr.2009.11.002
21. Thorat ND, Bohara RA, Malgras V, et al. Multimodal superparamagnetic nanoparticles with unusually enhanced specific absorption rate for synergetic cancer therapeutics and magnetic resonance imaging. *ACS Appl Mater Interfaces*. 2016;8(23):14656–14664. doi:10.1021/acsami.6b02616
22. Liong M, Shao H, Haun JB, et al. Carboxymethylated polyvinyl alcohol stabilizes doped ferrofluids for biological applications. *Adv Mater*. 2010;22(45):5168–5172. doi:10.1002/adma.201002219
23. Muthana M, Kennerley AJ, Hughes R, et al. Directing cell therapy to anatomic target sites in vivo with magnetic resonance targeting. *Nat Commun*. 2015;6:8009. doi:10.1038/ncomms9009
24. Xu C, Wang B, Sun S. Dumbbell-like Au-Fe3O4 nanoparticles for target-specific platin delivery. *J Am Chem Soc*. 2009;131(12):4216–4217. doi:10.1021/ja900790v
25. Huang J, Li Y, Orza A, et al. Magnetic nanoparticle facilitated drug delivery for cancer therapy with targeted and image-guided approaches. *Adv Funct Mater*. 2016;26(22):3818–3836. doi:10.1002/adfm.201504185
26. Mashhadi Malekzadeh A, Ramazani A, Tabatabaei Rezaei SJ, et al. Design and construction of multifunctional hyperbranched polymers coated magnetite nanoparticles for both targeting magnetic resonance imaging and cancer therapy. *J Colloid Interface Sci*. 2017;490:64–73. doi:10.1016/j.jcis.2016.11.014
27. Inozemtseva OA, German SV, Navolokin NA, et al. Encapsulated magnetite nanoparticles: preparation and application as multifunctional tool for drug delivery systems. *Nanotechnol Biosensors*. 2018;175–192.
28. Thiesen B, Jordan A. Clinical applications of magnetic nanoparticles for hyperthermia. *Int J Hyperthermia*. 2008;24(6):467–474. doi:10.1080/02656730802104757
29. Hu SH, Gao X. Nanocomposites with spatially separated functionalities for combined imaging and magnetolytic therapy. *J Am Chem Soc*. 2010;132(21):7234–7237. doi:10.1021/ja102489q
30. Tong S, Quinto CA, Zhang L, et al. Size-dependent heating of magnetic iron oxide nanoparticles. *ACS Nano*. 2017;11(7):6808–6816. doi:10.1021/acsnano.7b01762
31. Moroz P, Jones SK, Gray BN. The effect of tumour size on ferromagnetic embolization hyperthermia in a rabbit liver tumour model. *Int J Hyperthermia*. 2002;18(2):129–140. doi:10.1080/02656730110095609
32. Yanase M, Shinkai M, Honda H, et al. Antitumor immunity induction by intracellular hyperthermia using magnetite cationic liposomes. *Jpn J Cancer Res*. 1998;89(7):775–782. doi:10.1111/j.1349-7006.1998.tb03283.x
33. Tanaka K, Ito A, Kobayashi T, et al. Intratumoral injection of immature dendritic cells enhances antitumor effect of hyperthermia using magnetic nanoparticles. *Int J Cancer*. 2005;116(4):624–633. doi:10.1002/ijc.21061
34. Granov AM, Tiutin LA, Tarazov PG, et al. Modern technologies of diagnosis and combined surgical treatment in liver tumors. *Vestn Ross Akad Med Nau*. 2003;10:51–54.
35. Fang K, Song L, Gu Z, et al. Magnetic field activated drug release system based on magnetic PLGA microspheres for chemo-thermal therapy. *Colloids Surf B Biointerfaces*. 2015;136:712–720. doi:10.1016/j.colsurfb.2015.10.014
36. Xue W, Liu XL, Ma H, et al. AMF responsive DOX-loaded magnetic microspheres: transmembrane drug release mechanism and multimodality postsurgical treatment of breast cancer. *J Mater Chem B*. 2018;6(15):2289–2303. doi:10.1039/C7TB03206D
37. Gholami A, Mousavi SM, Hashemi SA, et al. Current trends in chemical modifications of magnetic nanoparticles for targeted drug delivery in cancer chemotherapy. *Drug Metab Rev*. 2020;52(1):205–224.
38. Peters T Jr. Serum albumin. *Adv Protein Chem*. 1985;37:161–245.
39. Albarqi HA, Wong LH, Schumann C, et al. Biocompatible nanoclusters with high heating efficiency for systemically delivered magnetic hyperthermia. *ACS Nano*. 2019;13(6):6383–6395. doi:10.1021/acsnano.8b06542
40. Mehrmohammadi M, Oh J, Mallidi S, et al. Pulsed magneto-motive ultrasound imaging using ultrasmall magnetic nanoprobes. *Mol Imaging*. 2011;10(2):102–110. doi:10.2310/7290.2010.00037

41. Boven E, van der Vijgh WJ, Nauta MM, et al. Comparative activity and distribution studies of five platinum analogues in nude mice bearing human ovarian carcinoma xenografts. *Cancer Res*. 1985;45(1):86–90.
42. Hashad RA, Ishak RA, Geneidi AS, et al. Methotrexate loading in chitosan nanoparticles at a novel pH: response surface modeling, optimization and characterization. *Int J Biol Macromol*. 2016;91:630–639. doi:10.1016/j.ijbiomac.2016.06.014
43. Akasaka K, Gyimesi-Forrás K, Lämmerhofer M, et al. Investigations of molecular recognition aspects related to the enantiomer separation of 2-methoxy-2-(1-naphthyl)propionic acid using quinine carbamate as chiral selector: an NMR and FT-IR spectroscopic as well as X-ray crystallographic study. *Chirality*. 2005;17(9):544–555. doi:10.1002/chir.20203
44. Tu TY, Yang SJ, Tsai MH, et al. Dual-triggered drug-release vehicles for synergistic cancer therapy. *Colloids Surf B Biointerfaces*. 2019;173:788–797. doi:10.1016/j.colsurfb.2018.10.043
45. Ishay RB, Israel LL, Eitan EL, et al. Maghemite-human serum albumin hybrid nanoparticles: towards a theranostic system with high MRI r2* relaxivity. *J Mater Chem B*. 2016;4(21):3801–3814. doi:10.1039/C6TB00778C
46. Rabin Y. Is intracellular hyperthermia superior to extracellular hyperthermia in the thermal sense? *Int J Hyperthermia*. 2002;18 (3):194–202. doi:10.1080/02656730110116713
47. Giustini AJ, Ivkov R, Hoopes PJ. Magnetic nanoparticle biodistribution following intratumoral administration. *Nanotechnology*. 2011;22 (34):345101. doi:10.1088/0957-4484/22/34/345101
48. Chen F, Tang F, Yang CT, et al. Fast and highly sensitive detection of pathogens wreathed with magnetic nanoparticles using dark-field microscopy. *ACS Sens*. 2018;3(10):2175–2181. doi:10.1021/acssensors.8b00785
49. Kato T, Jin CS, Ujiie H, et al. Nanoparticle targeted folate receptor 1-enhanced photodynamic therapy for lung cancer. *Lung Cancer*. 2017;113:59–68. doi:10.1016/j.lungcan.2017.09.002
50. Marinho LA, Rettori O, Vieira-Matos AN. Body weight loss as an indicator of breast cancer recurrence. *Acta Oncol*. 2001;40 (7):832–837. doi:10.1080/02841860152703454